RESEARCH ARTICLE

Human and rat brain lipofuscin proteome

Philipp Ottis[1], Katharina Koppe[1], Bruce Onisko[2,3], Irina Dynin[3], Thomas Arzberger[4], Hans Kretzschmar[4], Jesus R. Requena[5], Christopher J. Silva[3], Joseph P. Huston[6] and Carsten Korth[1]

[1] Department of Neuropathology, Heinrich Heine University of Düsseldorf, Düsseldorf, Germany
[2] OniPro, Kensington, CA, USA
[3] USDA, Albany, CA, USA
[4] Department Neuropathology, Ludwig-Maximilians-Universität München, München, Germany
[5] Department of Medicine and CIMUS Biomedical Research Institute, University of Santiago de Compostela-IDIS, Santiago, Spain
[6] Center for Behavioral Neuroscience, Department Experimental Psychology, Heinrich Heine University of Düsseldorf, Düsseldorf, Germany

Received: December 26, 2011
Revised: March 11, 2012
Accepted: March 26, 2012

The accumulation of an autofluorescent pigment called lipofuscin in neurons is an invariable hallmark of brain aging. So far, this material has been considered to be waste material without particular relevance for cellular pathology. However, two lines of evidence argue that lipofuscin may play a yet unidentified role for pathological cellular functions: (i) Genetic forms of premature accumulation of similar autofluorescent material in neuronal ceroid lipofuscinosis indicate a direct disease-associated link to lipofuscin; (ii) Retinal pigment epithelium cell lipofuscin is mechanistically linked to age-associated macular degeneration. Here, we purified autofluorescent material from the temporal and hippocampal cortices of three different human individuals by a two-step ultracentrifugation on sucrose gradients. For human brain lipofuscin, we could identify a common set of 49 (among > 200 total) proteins that are mainly derived from mitochondria, cytoskeleton, and cell membrane. This brain lipofuscin proteome was validated in an interspecies comparison with whole brain rat lipofuscin (total > 300 proteins), purified by the same procedure, yielding an overlap of 32 proteins (64%) between lipofuscins of both species. Our study is the first to characterize human and rat brain lipofuscin and identifies high homology, pointing to common cellular pathomechanisms of age-associated lipofuscin accumulation despite the huge (40-fold) difference in the lifespan of these species. Our identification of these distinct proteins will now allow research in disturbed molecular pathways during age-associated dysfunctional lysosomal degradation.

Keywords:
Aging / ATP synthase / Biomedicine / Fluorescence detection / Mitochondria / Oxidative phosphorylation

1 Introduction

Lipofuscin, first described in neurons by Hannover in 1842 [1] as a yellow-brown pigment, is found in postmitotic cells such as neurons, cardiac myocytes, retinal pigment epithelium (RPE) cells, and skeletal muscle fibers (reviewed in [2]). It appears chemically and morphologically polymorphous and, due to its assumed lysosomal origin, is widely considered to be waste material [3]. Lipofuscin consists of electron-dense material and features autofluorescence with characteristic spectral properties, showing emission at wavelengths between 460 and 630 nm when excited at wavelengths between 320 and 480 nm (Fig. 1) [4]. These pigment granules consist of approximately two-thirds protein and one-third lipids [5, 6]. Furthermore, small amounts of carbohydrates as well as traces of metal—mainly iron—have been reported to be contained in lipofuscin [5–7], while the lipid constituents

Correspondence: Dr. Carsten Korth, Neurodegeneration Unit, Department Neuropathology, University of Duesseldorf Medical School, Moorenstrasse 5, 40225 Duesseldorf, Germany.
E-mail: ckorth@uni-duesseldorf.de
Fax: +49-211-8117804

Abbreviations: AMD, age-associated macular degeneration; **HNE**, 4-hydroxy-2-nonenal; **MDA**, malondialdehyde; **NCL**, neuronal ceroid lipofuscinosis; **RPE**, retinal pigment epithelium

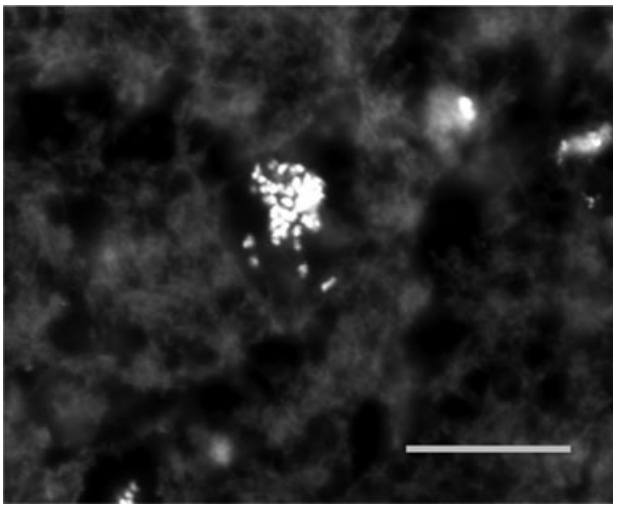

Figure 1. Fluorescent lipofuscin accumulation in a neuron of human brain (65 years). Cryosection of cortex under a fluorescence microscope with an excitation of 450–490 nm and detection at 520 nm. Visible are autofluorescent lipofuscin granules in a cortical neuron. Scale bar 20 μm.

have been characterized as triglycerides, free fatty acids, cholesterol, phospholipids, dolichols, and phosphorylated dolichols [3].

So far, most research into lipofuscin has focused on RPE-lipofuscin. The proteomic content of RPE lipofuscin has been investigated [8, 9] and retinoid derivatives were reported in these lipopigments [10]. In contrast, for the analysis of brain lipofuscin, only candidate protein identification rather than a systematic proteomic analysis has been performed. For example, amyloid β-protein was detected in neuronal lipofuscin [11]. The presence of undegraded macromolecules derived from phagocytosed long-lived proteins and damaged organelles, mainly mitochondria, appears to be a common feature of these lipopigments [8, 9, 12–14].

Lipofuscin, often referred to as "aging pigment," is located primarily in secondary lysosomes or residual bodies of post-mitotic cells [15–17] and accumulates in a linear relation to age [18–20]. For human myocardial cells, an accumulation of approximately 0.067% pigment growth per year and cell volume was determined [20] and for canine myocardium and the nervous system of *Callinectes sapidus* (blue crabs) such a correlation with age has also been shown [18, 19]. Lipofuscin is, therefore, considered to be a hallmark of aging. It has been difficult to ascribe a pathogenetic role for lipofuscin in physiological aging and, amazingly, lipofuscin accumulation adding up to 75% of the soma volume in aged neurons is still not considered to be abnormal [2]. Furthermore, the varying amount of lipofuscin accumulation in different neuronal subtypes remains unexplained [21].

The current concept of how lipofuscin originates [22] is that intracellular macromolecules and organelles such as mitochondria, destined for lysosomal degradation, get engulfed by a membranous phagophore in a phagocytotic process, resulting in the formation of an autophagosome. Extracellular material is taken up by phagocytosis, forming an early endosome. Fusion of these organelles with vesicles from the trans-Golgi network or with a mature resting lysosome delivers the proteolytic lysosomal enzymes together with an acidic environment, resulting in the formation of an autolysosome and in the degradation of the enclosed molecules. In a perfect process, this would result in complete degradation of the engulfed material, yielding an "empty" mature, resting lysosome. However, in the case of lipofuscin, lysosomal degradation is incomplete, leaving behind undegradable material that is not exocytosed and accumulates in the lysosomes over time (reviewed in ref. [22]).

Lipofuscin-like material present in genetic forms of premature lipopigment accumulation, termed neuronal ceroid lipofuscinoses (NCLs), is called ceroid and clearly has to be distinguished by nomenclature from mere age-related lipofuscin, as ceroids are not age-associated, but occur prematurely as a result of genetic mutational diseases (e.g. NCLs) [4, 23–26].

Purified lipofuscin granules have been demonstrated to show biological effects: Studies conducted with nonpathological lipofuscin-loaded cells, or cells treated with exogenous, purified lipofuscin granules, report a decrease in lysosomal hydrolase activity, antioxidant enzymes, and glutathione levels in those cells [27]. These experiments suggest a subsequent decay of the cells' capability to cope with potential stress factors will eventually lead to reduced viability and oxidative stress-induced apoptosis [28]. These studies, combined with our understanding of the role of RPE lipofuscin in age-associated macular degeneration (AMD) [29], suggest that the presence of lipofuscin is indicative of more than just a benign accumulation of "cellular garbage."

We hypothesized that due to the linear increase in the accumulation of lipofuscin with age, its pathogenic role in AMD and genetic NCLs, an analysis of the lipofuscin proteome might reveal candidate proteins involved in or hinting at the cellular circuitry that is deficient in the lysosomal failure during lipofuscin generation. Here, we analyzed the proteomic composition of human brain lipofuscin in three independent samples and validated this analysis by the analysis of rat brain lipofuscin.

2 Material and methods

2.1 Tissue

Animal brain tissue derived from whole brains of seven 20- to 21-month-old Wistar rats. Rats were anesthetized by inhalation of carbon dioxide directly before termination by decapitation and subsequent brain removal. For the first experiment (in the following depicted as "rat A"), the brain tissue of five rats was briefly kept on ice, pooled, and, subsequently homogenized and subjected to lipofuscin purification. The two remaining rat brains were snap-frozen in liquid nitrogen

directly after removal and were stored at –80°C until they were separately homogenized and subjected to lipofuscin purification.

Human brain tissue was obtained via the European BrainNet with informed consent and with consideration of all relevant ethical issues (outlined on http://www.brainnet-europe.org). In addition, experimentation with human brain tissue was approved by the Ethics Committee of the Medical Faculty of the University of Düsseldorf (#1978/2002 and 3224/2009).

The brains underwent a thorough neuropathological exam which led to the neuropathological diagnosis of beginning Alzheimer's disease in one case (human A) or the complete absence of brain disease (human B, human C). "Human brain A" was from temporal cortex of a 64-year-old female individual where the occurrence of neurofibrillary tangles at Braak stage IV had been noted [30] and CERAD-grade C was determined [31]. Human brain samples B and C were pieces of gyrus parahippocampalis from two female subjects, 85 years and 83 years old, respectively. Human B was noted to show no amyloid plaques and was classified Braak stage I. Human C was noted to show a few plaques in the gyrus hippocampalis and was classified Braak stage II. Both, human B and human C, were assigned the CERAD-grade 0. No other brain pathology or clinical disease was reported for the human samples.

2.2 Lipofuscin purification

All experimental steps were carried out on ice with prechilled buffers. All centrifugation steps were performed at 4°C. Lipofuscin was isolated using a method described by Boulton and Marshall [32]. Briefly, the deep frozen or fresh brain tissue was homogenized in presence of VRL buffer (50 mM Hepes, 0.25 M sucrose, 5 mM EDTA, 0.1 M potassium acetate, pH 7.5) supplemented with protease inhibitors (cOmplete, EDTA-free Protease Inhibitor Cocktail Tablets/Roche Applied Science, Mannheim, Germany) in a Dounce homogenizer to yield a 20% homogenate. The homogenate was centrifuged at 60 × *g* for 7 min. The resulting supernatant was removed and then centrifuged (6000 × *g*; 10 min). The pellet was resuspended in VRL-buffer (0.7 mL per gram of brain tissue). The suspension was layered on top of a discontinuous gradient consisting of five different concentrations of sucrose in VRL-buffer: 1.6, 1.5, 1.4, 1.2, 1.0 M. One large-scale preparation (rat A: 1, 1.2, 1.4 M, 5 mL each; 1.5, 1.6, 1.8 M, 3.5 mL each; human A: 1, 1,2, 1.4 M, 7 mL each; 1.5, 1.6 M, 3.5 mL each) and two small-scale preparations were performed (human B, C, rat B, C: each sucrose fraction was 0.75 mL and sample was 0.7 mL. All in a 5-mL Eppendorf ultracentrifugation tube).

Gradient separation was achieved by centrifugation at 100 000 × *g* for 1 h in a swing-bucket rotor (MLS-50, Beckman Coulter, Fullerton, CA, USA). The lipofuscin-containing interface was identified by its characteristic fluorescence excitation/emission spectrum [9, 32] (Fig. 2). The lipofuscin-containing interface fraction was diluted with phosphate-buffered saline (PBS) and pelleted at 6000 × *g* for 10 min. The pellet was resuspended in VRL-buffer and a second gradient separation with subsequent fluorescence 3D-scans of the interfaces was performed as described above. Finally, the identified lipofuscin fraction was diluted with PBS, pelleted, and washed two times in PBS (all 6000 × *g*; 10 min).

2.3 Fluorescence 3D scans

Identification of the lipofuscin-containing fractions was achieved by analyzing the excitation wavelengths and emission spectra of the different samples. This was performed in a Safire microplate reader (Tecan, Switzerland) using black 96-well microtiter plates. Emission spectra were recorded between 400 and 500 nm for the excitation wavelengths: 325, 340, 355, 365, 370, 375, 385 nm (Fig. 2).

2.4 SDS-PAGE 1D-separation and sampling

Purified and washed lipofuscin, derived from 0.75 g brain tissue, was mixed with SDS-loading buffer supplemented with 1% beta-mercaptoethanol, heated to 95°C for 5 min, and was loaded onto an SDS gel. Separation of the polypeptides was achieved by electrophoresis with application of 180 V for approximately 1 h. Following this, the gel was stained for proteins with the Colloidal Blue Staining Kit (Invitrogen, Darmstadt, Germany; see Supporting Information Figs. S1–S4). The resulting visualized smear of proteins was excised from the gel and was cut into small gel bands. The excised bands were cut into 1 mm sized cubes, placed in 96-well digestion trays (INTAVIS Bioanalytical Instruments AG, Bergisch Gladbach, Germany) according to their apparent molecular weight in the gel. Subsequently, these gel cubes were subjected to in-gel trypsin digestion.

2.5 In-gel digestion and processing of peptides

In-gel digestion of the 96-well digestion trays was done with a DigestPro (INTAVIS Bioanalytical Instruments AG, Koeln, Germany). Following washing, reduction with DTT, alkylation with iodoacetamide, and tryptic digestion, the peptides were eluted with 40 μL of 10% formic acid containing 0.1% trifluoroacetic acid.

2.6 LC/MS/MS

NanoLC/ESI/MS/MS analysis for human B, C, and rat B, C samples was done with an Applied Biosystems (ABI/MDS SCIEX, Toronto, Canada) model QStar Pulsar equipped with a Proxeon Biosystems (Odense, Denmark) nanoelectrospray source. Digested samples (20 μL) were loaded automatically

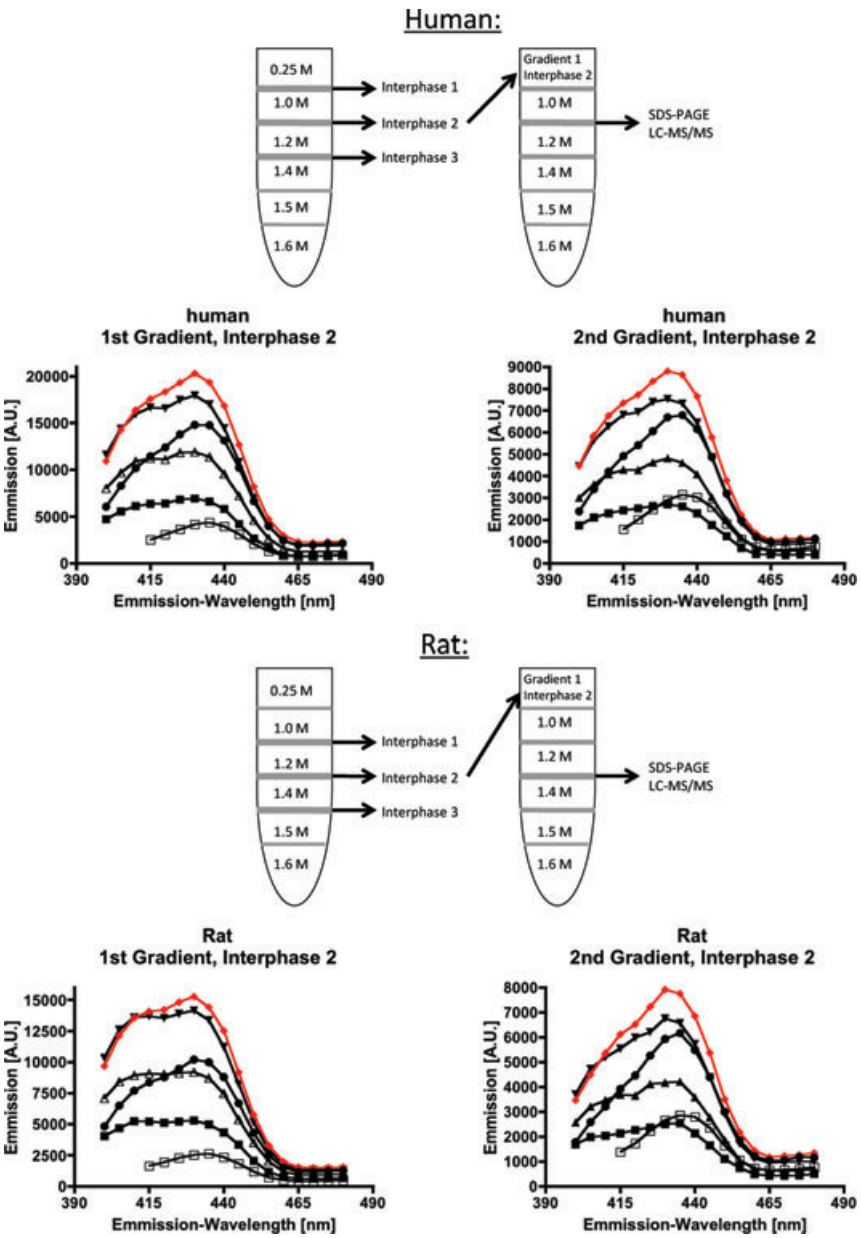

Figure 2. Flowchart of lipofuscin purification by sucrose gradients out of human (top panel) and rat (bottom panel) brain homogenates, as well as 3D fluorescence scans of selected lipofuscin fractions. A schematic tube with layers consisting of discontinuous sucrose concentrations is shown on top of both panels. Below are the fluorescence scans for human and for rat lipofuscin fractions showing emission spectra at variable excitation wave lengths for the first and the second sucrose gradient. The second purification step led to a reduction in fluorescence intensity of the selected fraction approximately 50%. Characteristic emission maximum with 370 nm excitation is highlighted in red. In each of the 3D fluorescence scans, the emission spectra of the following excitation wavelengths are depicted: Filled squares 325 nm, open triangles 340 nm, filled triangles 355 nm, filled red diamonds 370 nm, black diamonds 385 nm, open squares 400 nm.

onto a C-18 trap cartridge and chromatographed on a RP column (EASY-Column, 75 μm × 100 mm; Thermo Scientific; Waltham, MA, USA) fitted at the effluent end with stainless steel emitter spray tip (Thermo Scientific). A nanoflow LC system (EASY-nLC II, Thermo Scientific) with autosampler, column-switching device, loading pump, and nanoflow solvent delivery system was used. Elution solvents were A (0.1% formic acid in water) and B (0.1% formic acid in ACN). Samples were eluted at 250 nL/min with the following gradient profile: 15% B at 0 min to 25% B in a 25-min linear gradient; 45% B at 25 min to 60% B in a 5-min linear gradient; 60% B at 30 min to 80% B in a 5-min linear gradient; held at 80% B for 5 min then back to 15% B for 5 min. The QStar Pulsar was externally calibrated daily and operated above a resolution of 8000. The acquisition cycle time of 6 s consisted of a single 1-s MS "survey" scan followed by a 5-s MS/MS scan. Ions between m/z 400 and 2500 of charge states between +2 and +4 having intensities greater than 40 counts in the survey scan were selected for fragmentation to improve spectra quality. A new 1-s survey scan was then repeated to find the next best precursor for MS/MS. The dynamic exclusion window was set to exclude previously fragmented masses for the next 45 s to prevent repeated MS/MS analysis of the same peptide, but to allow other peptides with similar precursors, but different retention times to be analyzed. Collision energy optimized for charge state and m/z was automatically selected by the Analyst QS software after adjusting parameters to obtain satisfactory fragmentation of human [Glu^1]-fibrinopeptide B (+2).

Nitrogen was used for the collision gas, and the pressure in the collision cell ranged from 3×10^{-6} to 6×10^{-6} torr.

In between the analysis of human A/rat A samples and the respective B and C samples, the nanoLC-system had to be replaced; therefore, the gradient settings were slightly different. Elution solvents for the A samples were A (0.5% acetic acid in water) and B (0.5% acetic acid in 80% ACN/20% water) in a 15-min linear gradient from 2% B at 0 min to 80% B, held at 80% B for 5 min, returned to 2% B over 10 min from a RP column (Vydac, Grace Davison Discovery Sciences, Deerfield, IL, 238EV5.07515, 75 μm × 150 mm) fitted with a coated spray tip (FS360–50-5-CE; New Objective, Inc., Woburn, MA). NanoLC ESI MS/MS was done with an AB QStar Pulsar, with a Proxeon Biosystems nano-electrospray source, with resolution >10 000. A 5-s MS/MS scan followed a 1-s survey scan. Ions between m/z 400 and 1000, charges between +2 and +5, and intensities >40 counts were fragmented.

2.7 Database searching

MS/MS spectra were extracted in a deconvoluted and deisotoped charge state by Analyst QS version 1.1. All MS/MS samples were analyzed using Mascot (Matrix Science, London, UK; version Mascot) and X! Tandem (The GPM, thegpm.org; version CYCLONE [2010.12.01.1]). Mascot was set up to search the human or rat subset of the UniProt-database [33]. X! Tandem was set up to search the subset databases (state: June 2011, 41 471 entries for human and 33 954 entries for rat), assuming a digestion of the proteins with trypsin. Conducting the searches Mascot and X! Tandem allowed for fragment ion mass tolerance of 0.100 Da and a parent ion tolerance of 0.200 Da. The iodoacetamide derivative of cysteine was specified in Mascot and X! Tandem as a fixed modification, whereas oxidation of methionine was specified as a variable modification.

2.8 Criteria for protein identification

Scaffold (version Scaffold_3.2.0, Proteome Software Inc., Portland, OR, USA) was used to validate MS/MS-based peptide and protein assignments. Peptide identifications were accepted if they could be established at greater than 95.0% probability as specified by the Peptide Prophet algorithm [34]. Protein identifications were accepted if they could be established at greater than 99.9% probability and included at least three different identified peptides. Protein probabilities were assigned by the Protein Prophet algorithm [35]. Proteins that contained similar peptides and could not be differentiated based on MS/MS analysis alone were grouped to satisfy the principles of parsimony.

2.9 Data analyses

Detected proteins were checked for probability with regard to their approximate molecular weight observed in the gel and the amount of the corresponding peptides together with the resulting total sequence coverage. Peptides matched to unidentified proteins were manually reinvestigated for fitting to other known polypeptides. Fully uncharacterized proteins, whose peptides could not be mapped to other characterized proteins, were excluded from the final listing.

Gene ontology (GO) analyses were performed using the online DAVID Bioinformatics Resources 6.7 tool [36, 37] applying a brain subset of human or rat UniProt database [33] as background. *p*-Values stated were calculated by the DAVID tool and were corrected according to Bonferroni.

3 Results

3.1 Identifying lipofuscin guided by its fluorescence characteristics in sucrose gradients

Lipofuscin was purified from brain homogenates using the methods of Boulton and Marshall [32], and Schutt et al. [9]. The presence of the lipofuscin fractions was revealed by their characteristic fluorescent excitation using 3D-fluorescence scans. (Fig. 2) [8, 9].

After each ultracentrifugation step for both rat and human samples, three articulate interfaces formed, with the topmost containing a brown flocculent suspension. For the human samples, this fraction did not enter the gradient, but was present between the sample and the 1.0 M sucrose fraction (Fig. 2). For the rat sample, that upper interface formed between 1.0 and 1.2 M sucrose. Though this fraction had the highest emission maxima in the fluorescence scans for some of the samples, this interface presumably consisted to a large proportion of lipids and cell debris that was not readily separated by the gradient. Therefore, it was not analyzed further. The middle and lower interfaces are formed between 1.0 and 1.2 M sucrose, and between 1.2 and 1.4 M for the human samples. For the rat samples, they are formed between 1.2 and 1.4 M, and between 1.4 and 1.5 M. With the middle interface giving the highest characteristic emission maximum at 430 nm with 370 nm excitation wavelength (Fig. 2), these fractions at 1.0 M/1.2 M for human and 1.2 M/1.4 M for rat samples, respectively, were subjected to a second purification step on the same sucrose gradient.

After the second ultracentrifugation, the same interfaces as in the first gradient, 1.0 M/1.2 M (human), and 1.2 M/1.4 M (rat), respectively, were processed further (Fig. 2). These fractions were then washed, concentrated, separated via SDS-PAGE, and analyzed by MS as described.

Figure 2 displays representative plots of 3D-fluorescence-scans performed on those lipofuscin gradient interfaces used for further processing. Apparent are the emission maxima at 430 nm that reach their peak at an excitation wavelength of 370 nm. These observed spectra are consistent with the reported characteristics of lipofuscin granules isolated from RPE cells by Schutt et al. [9] and indicated purity.

Table 1. Major human brain lipofuscin proteins.

Entry Human	Entry Rat	Protein name	Subcellular location
P62258		14–3-3 protein epsilon	Cytoplasm/Melanosome
P61981		14–3-3 protein gamma (Protein kinase C inhibitor protein 1)	Cytoplasm
P63104	**P63102**	14–3-3 protein zeta/delta (Protein kinase C inhibitor protein 1)	Cytoplasm/Melanosome
P09543	**P13233**	2′,3′-cyclic-nucleotide 3′-phosphodiesterase	Cytoplasm/ Melanosome/Membrane
P10809	**P63039**	60 kDa heat shock protein, mitochondrial	Mitochondrion
***P60709**	**P60711**	Actin, cytoplasmic 1 (Beta-actin)	Cytoplasm/Cytoskeleton
*P02511		Alpha-crystallin B chain (Heat shock protein beta-5)	Cytoplasm
***P25705**	**P15999**	ATP synthase subunit alpha, mitochondrial	Mitochondrion/Membrane
***P06576**	**P10719**	ATP synthase subunit beta, mitochondrial	Mitochondrion/Membrane
*O75947	**P31399**	ATP synthase subunit d, mitochondrial	Mitochondrion/Membrane
P48047	**Q06647**	ATP synthase subunit O, mitochondria	Mitochondrion/Membrane
P80723		Brain acid soluble protein 1	Cell membrane
Q9UQM7		Calcium/calmodulin-dependent protein kinase type II subunit alpha	Synapse
Q00610		Clathrin heavy chain 1	Cytoplasm/Vesicle/Membrane
***P12277**	**P07335**	Creatine kinase B-type	Cytoplasm
P12532		Creatine kinase U-type, mitochondrial	Mitochondrion/Membrane
*P20674	**P11240**	Cytochrome c oxidase subunit 5A, mitochondrial	Mitochondrion/Membrane
Q16555	P47942	Dihydropyrimidinase-related protein 2	Cytoplasm
Q05193		Dynamin-1	Cytoplasm
*P09104	P07323	Gamma-enolase (Neuron-specific enolase)	Cytoplasm/Membrane
*P14136		Glial fibrillary acidic protein (GFAP)	Cytoplasm
***P04406**	**P04797**	Glyceraldehyde-3-phosphate dehydrogenase (GAPDH)	Cytoplasm
P62873	**P54311**	Guanine nucleotide binding protein G(I)/G(S)/G(T) subunit beta-1	Cell membrane
*P09471	**P59215**	Guanine nucleotide binding protein G(o) subunit alpha	Cell membrane
Q08722		Leukocyte surface antigen (CD antigen CD47)	Cell membrane
Q13449		Limbic system associated membrane protein (LSAMP)	Cell membrane
*O75489		NADH dehydrogenase [ubiquinone] iron-sulfur protein 3, mitochondr.	Mitochondrion/Membrane
P07196		Neurofilament light polypeptide (NF-L)	Cytoplasm
P62937	**P10111**	Peptidyl-prolyl cis-trans isomerase A (PPIase A)	Cytoplasm
P13637	**P06687**	Sodium/potassium-transporting ATPase subunit alpha-3	Cell membrane
Q13813	**P16086**	Spectrin alpha chain, brain	Cytoplasm
Q01082	Q6XD99	Spectrin beta chain, brain 1	Cytoplasm
P60880	P60881	Synaptosomal-associated protein 25 (SNAP-25)	Synapse/Membrane
P61266	**P61265**	Syntaxin-1B	Cell membrane
P61764	**P61765**	Syntaxin-binding protein 1	Cytoplasm/Vesicle/Membrane
P04216	**P01830**	Thy-1 membrane glycoprotein (CD antigen CD90)	Cell membrane
P60174	**P48500**	Triosephosphate isomerase (TIM)	Cytoplasm
***P68363**	**Q6P9V9**	Tubulin alpha-1B chain	Cytoplasm/Cytoskeleton
P68366	Q5XIF6	Tubulin alpha-4A chain	Cytoplasm/Cytoskeleton
***Q13885**	**P85108**	Tubulin beta-2A chain	Cytoplasm/Cytoskeleton
***P68371**	**Q6P9T8**	Tubulin beta-2C chain	Cytoplasm/Cytoskeleton
***Q13509**		Tubulin beta-3 chain	Cytoplasm/Cytoskeleton
*P04350		Tubulin beta-4 chain	Cytoplasm/Cytoskeleton
*P07437		Tubulin beta-5 chain	Cytoplasm/Cytoskeleton
O94811		Tubulin polymerization-promoting protein (25 kDa, brain-specific)	Cytoplasm
P09936	Q00981	Ubiquitin carboxyl-terminal hydrolase isozyme L1	Cytoplasm
P36543	Q6PCU2	V-type proton ATPase subunit E 1	Cytoplasm/Vesicle/Membrane
P63027	**P63045**	Vesicle-associated membrane protein 2 (VAMP-2)	Cytoplasm/Vesicle/Membrane
***P21796**	Q9Z2L0	Voltage-dependent anion-selective channel protein 1	Mitochondrion/Membrane

Only those proteins that were identified in at least two of three independent analyses of human lipofuscin are depicted. Human orthologs, having been detected in at least two of three independent analyses of rat lipofuscin, are indicated by listing of the rat accession number. Proteins identified in all three experiments for human and for rat are highlighted in bold. Polypeptides, identified in RPE-derived human lipofuscin in the study conducted by Schutt et al. in 2002 [9], are marked with an asterisk.

3.2 Validation of human lipofuscin proteome content by intra- and interspecies comparisons

The initial experiment with "human A" and "rat A" brain samples employed three SDS gels of different acrylamide content (7.5%, 4–15%, 4–20%) in order to identify the best resolution for lipofuscin proteins and to enable detection of low-abundance proteins. By combining the MS/MS data of all peptides identified in the three different gels, we were able to identify 175 proteins for "human A" and 205 proteins for "rat A" (Supporting Information Tables S1 and S2). In order to validate the more abundant proteins as being the key players in lipopigment composition, two further experiments using MS/MS analysis of purified lipofuscin were performed for human ("human B" and "human C") and for rat ("rat B" and "rat C") samples. Here, only one gel (4–12% acrylamide) was used to separate the samples' proteins. This resulted in the clear identification of 33 proteins for "human B" and 49 proteins for "human C." For the rat samples, 57 lipofuscin-derived proteins could be identified in "rat B" and 66 in "rat C" (Supporting Information Table S2). Keratins and myelin-related proteins were excluded from the protein listings shown, as they are most likely contaminants and impurities that co-sediment with the pigment granules. Only proteins identified in at least two of the three experiments performed per species were considered to be validated and, therefore, are presented here as possible lipofuscin components (Table 1). The Venn diagrams in Fig. 3 visualize the amount of proteins identified in multiple samples and across species in rat and human lipopigments. Within the human triplicate analysis, 29 proteins were identified in two of the three experiments and 20 were found to be present in all human samples, together accounting for 49 proteins detected in more than two analyses of human lipofuscin. For the rat analyses, 27 proteins could be confirmed to be present in all three data sets, whereas 35 were identified in two separate experiments. Hence, a total of 62 rat proteins detected could be verified in at least one additional approach. The lower two diagrams in Fig. 3 display the overlap of lipofuscin proteins present in human and rat.

3.3 Analysis of validated top protein hits in human brain lipofuscin

All human proteins identified in at least two experiments are listed in Table 1 alongside the rat orthologs. Although most proteins could be identified at approximately the expected height in the gels with best sequence coverage, many proteins were found in clusters appearing at various positions in the gels, presumably due to crosslinking and different proteolytic processing. It is believed that uncontrolled oxidation within lipofuscin granules favors intermolecular crosslinking [22, 38]. GO analysis of the human proteins in Table 1 highlighted the significant enrichment ($p = 0.01$) of proteins of the mitochondrial membrane together with the 60 kDa heat shock protein, mainly located in the mitochondrial matrix. Apart from this heat shock protein and the voltage-dependent anion-selective channel protein 1 in the outer mitochondrial membrane, this protein cluster is composed of the U-type creatin kinase and subunits of the ATP synthase, of NADH dehydrogenase (Complex I), and of cytochrome c oxidase. All these subunits are part of the mitochondrial oxidative phosphorylation pathway.

Another identified cluster contains the cytoskeleton proteins beta-actin, together with tubulin alpha and beta chains, the intermediary filaments glial fibrillary acidic protein (GFAP) and neurofilament light polypeptide (NFL), as well as polypeptides associated with the cytoskeleton in terms of its maintenance and stability (tubulin polymerization promoting protein), remodeling (dihydropyrimidase-related protein 2), movement (spectrin alpha and beta chain), and transport (dynamin).

4 Discussion

To our knowledge, this is the first description of the proteomic composition of brain lipofuscin purified from human and rat brain. We validated our results by running several independent within-species analyses, as well as analyses of another species (rat). We used lipofuscin's characteristic autofluorescence to guide our purification, an approach previously employed to isolate RPE lipofuscin [8, 9]. This purification method relies on the integrity of binding of the autofluorescent pigments to the other proteins and it is not clear how strong this is; therefore, for further experiments focusing on the proteome content of brain lipofuscin, it would be helpful to have additional protein markers independent of the poorly defined autofluorescent brain lipofuscin pigments. One goal of the present study was to present lipofuscin protein candidates worth further investigation in future experiments to assess their value as autofluorescence-indpendent, tracking markers for brain lipofuscin.

The distribution of fractions formed during the separation of the homogenates in the sucrose gradient differed between human and rat. The fractions with the strongest characteristic excitation/emission spectra appeared to be shifted in their different sedimentation characteristics (by 0.2 M sucrose) toward heavier fractions in rat samples, even though the fluorescence characteristics of these interfaces were equal. These differences could be caused by different sizes of lipofuscin particles or differences in their relative lipid content, with a higher lipid content increasing buoyancy. For example, species differences in myelin content have been described to correlate with brain size, with bigger brains having higher myelin content [39], consistent with the increased buoyancy of human lipofuscin (Fig. 2).

We identified mitochondrial and cytoskeletal polypeptides as the main clusters of proteins present in neuronal lipofuscin. The proteome of retinal (RPE) lipofuscin had been identified previously [9] and in our data on brain lipofuscin, 19 of the 49 proteins (38%) listed in Table 1 were identical (marked with an asterisk in the table). Disregarding the

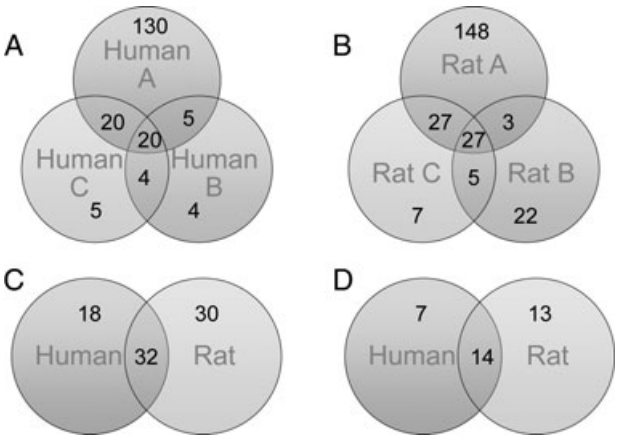

Figure 3. Venn diagrams of overlapping proteomic identification results. Values indicate the number of proteins clearly identified in each experiment. (A) Interrelation of the results for human lipofuscin with the three experiments Human A, B, and C. (B) Interrelation of the results for rat lipofuscin with the three experiments Rat A, B, and C. (C) Cross species overlap of proteins identified in at least two separate experiments for human and for rat. (D) Cross species overlap of proteins identified in all three separate experiments for human and for rat.

proteins of the visual cycle being present in RPE-lipopigments, the similarity of proteins indicates the existence of a general mechanism involved in lipofuscin formation. However, the fact that RPE lipofuscin is toxic and causes AMD whereas brain lipofuscin is at least not overtly neurotoxic to the brain suggests that either remaining differences in their protein, lipid, other organic or inorganic contents, or that different cellular susceptibility is responsible for the differences in the effects of accumulating lipofuscin.

The likelihood of general mechanisms of lipofuscin deposition is also highlighted by our findings of a 64% overlap of proteins clearly identified in both, human and rat, and also independent of Alzheimer disease neuropathology (present in the brain of human A). In particular, a majority of the polypeptides assigned to the two prominent protein clusters were shown to be present in neuronal lipofuscin of both species. On an absolute time scale, lipofuscin in humans appears much later in humans than it does in rats and the absolute age of neurons from rat and from human brain differed by a factor of 30–40 (investigated rat age: 21 months versus investigated human age: 64–85 years). The high similarity between human and rat lipofuscin protein content despite the large absolute time difference therefore indicates that that lipofuscin is likely to arise through distinct cellular processes rather than simple accumulation as a function of time and suggests a similarity in the still unknown age-associated lysosomal failure during brain aging in both species.

Many of the detected proteins were found at various positions in the gel and often also in high molecular weight fractions. Similar results were observed for the RPE pigments [9]. This indicates that those proteins were further processed by directed posttranslational modifications, proteolytic progression, and other undirected modifications occurring in the course of lipofuscin formation and deposition. Such undirected modifications may be, apart from oxidation [40], the attachment of advanced glycosylation end-products (AGEs) [41–43], modifications by malondialdehyde (MDA) and by 4-hydroxy-2-nonenal (HNE) [43, 44]. The latter two modifying components, MDA and HNE, are very reactive electrophilic aldehydes capable of crosslinking lysine residues and other primary amines. Both MDA and HNE are products of the reactive oxygen species (ROS) induced peroxidation of polyunsaturated lipids [44, 45] and around 40% of the hits reported for RPE-lipofuscin have been demonstrated to show MDA immunoreactivity [43]. In general, oxidative stress has been proposed to be the major trigger in lipofuscin formation [46]. ROS (primarily hydrogen peroxide) are mainly generated by mitochondria as byproducts of imperfect oxidative phosphorylation. They are assumed to diffuse into the lysosomes where they react with accumulated ferrous iron, Fe (II), in a Fenton-like reaction to generate highly reactive oxygen radicals, such as the hydroxyl radical, which then react with lipids to yield MDA and HNE or directly react with proteins present in the lysosome (reviewed by the group of Ulf T. Brunk [22, 38]). In addition, senescent mitochondria, producing increased amounts of ROS, have been proposed to accumulate in aged postmitotic cells, and thus, to act as the major cause of aging itself in these cells [38].

Curiously, many of the identified polypeptides are so-called housekeeping proteins. So far, most of these housekeeping proteins have not been shown to have any cytotoxic properties. Therefore, it has to be assumed that the reported toxic and stress-inducing effects of lipofuscin are related to the induced modifications occurring in the process of lipofuscin formation, as suggested by Schutt et al. [9]. However, there have been demonstrations of very abundant housekeeping genes showing important, previously unconsidered cellular functions. For example, the glyceraldehyde-3-phosphate dehydrogenase (GAPDH) was identified in all six experiments conducted here. This abundant protein, widely known for its role in the glycolytic pathway, was recently demonstrated to be involved in regulating apoptosis [47] in an aggregation-dependent manner and in oxidative stress induced cell death [48].

It should be noted that a proportion of our identified proteins is found among the top hits continuously reported in the majority of proteomic studies [49]. This especially applies to the various forms of tubulins and actin, but also to the 14–3-3 protein family and ATP synthase beta chain. However, in the case of brain lipofuscin, the group of ATP synthase subunits detected together with other proteins of the mitochondrial inner membrane indicates the specificity of these proteins as components of lipofuscin.

ATPase has been previously identified as a principal target of ROS-induced protein oxidative damage in rat liver mitochondria; in particular, as a target of oxidative modification by HNE [50]. In brain, it has been identified as a prominent target of modification by MDA [51]. Furthermore, an

age-related increase of oxidized ATP synthase has been found in interfibrillar heart mitochondria of rats [52].

While many of the proteins identified in neuronal lipofuscin in human and rat brain appear to be abundant housekeeping proteins, there is a striking overlap of the most prominent protein cluster of mitochondrial oxidative phosphorylation with the main components of pathologic ceroids reported for the genetic forms of premature lipofuscin-accumulation, the NCLs. The main components are ATP synthase subunit c and cytochrome c oxidase subunit 4 [23, 53, 54]. Even though these specific subunits could not be detected in our analyses, it remains highly intriguing that these polypeptides belong to the same protein complexes we identified as being the most prominent group in our data sets. This becomes even more interesting, considering that the symptoms observed in most of the NCLs, such as psychomotorical and cognitive impairments [4, 23], are also symptoms strongly associated with the "pathology" of aging. Hence, these findings may imply that ceroids in NCLs and lipofuscin in normal aging are not that different and they might share the same principle involved in the accumulation of nondegradable material affecting cell viability. It also supports the emerging view that lipofuscin is not just inert waste material, but, that on the contrary, it resembles ceroid accumulations, at least in part contributing to the pathology of NCLs, which, in turn, shares features also seen in the course of normal aging.

Further investigations regarding the proteomic composition of pathological ceroids versus age-associated lipopigments in the brain, the organ most susceptible to toxicity and oxidative stress, together with appropriate cell-culture models will help to contribute to the study of both lipopigment granules and their respective effects on the cell.

This research has been funded by grant from the EU-FP7 PRIORITY to C. K. and J. R. R., and grants form the DFG (GRK1033) and KNDD-Demtest to C. K., and Hu 306/27-2 to J.P.H.

The authors have declared no conflict of interest.

5 References

[1] Hannover, A., Mikroskopiske undersögelser af nervesystemet. *Kgl. Danske Vidensk. Kabernes Selskobs Naturv. Math. Afh. (Copenhagen)* 1842, *10*, 1–112.

[2] Terman, A., Brunk, U. T., Lipofuscin, Mechanisms of formation and increase with age. *APMIS* 1998, *106*, 265–276.

[3] Brunk, U. T., Terman, A., Lipofuscin, Mechanisms of age-related accumulation and influence on cell function. *Free Radic. Biol. Med.* 2002, *33*, 611–619.

[4] Seehafer, S. S., Pearce, D. A., You say lipofuscin, we say ceroid: defining autofluorescent storage material. *Neurobiol. Aging* 2006, *27*, 576–588.

[5] Jolly, R. D., Douglas, B. V., Davey, P. M., Roiri, J. E., Lipofuscin in bovine muscle and brain: a model for studying age pigment. *Gerontology* 1995, *41*(Suppl. 2), 283–295.

[6] Porta, E. A., Advances in age pigment research. *Arch. Gerontol. Geriatr.* 1991, *12*, 303–320.

[7] Essner, E., Novikoff, A. B., Human hepatocellular pigments and lysosomes. *J. Ultrastruct. Res.* 1960, *3*, 374–391.

[8] Warburton, S., Southwick, K., Hardman, R. M., Secrest, A. M. et al., Examining the proteins of functional retinal lipofuscin using proteomic analysis as a guide for understanding its origin. *Mol. Vis.* 2005, *11*, 1122–1134.

[9] Schutt, F., Ueberle, B., Schnölzer, M., Holz, F. G. et al., Proteome analysis of lipofuscin in human retinal pigment epithelial cells. *FEBS Lett.* 2002, *528*, 217–221.

[10] Murdaugh, L. S., Avalle, L. B., Mandal, S., Dill, A. E. et al., Compositional studies of human RPE lipofuscin. *J. Mass Spectrom.* 2010, *45*, 1139–1147.

[11] Bancher, C., Grundke-Iqbal, I., Iqbal, K., Kim, K. S. et al., Immunoreactivity of neuronal lipofuscin with monoclonal antibodies to the amyloid beta-protein. *Neurobiol. Aging* 1989, *10*, 125–132.

[12] Elleder, M., Sokolová, J., Hrebícek, M., Follow-up study of subunit c of mitochondrial ATP synthase (SCMAS) in Batten disease and in unrelated lysosomal disorders. *Acta. Neuropathol.* 1997, *93*, 379–390.

[13] Gray, D. A., Woulfe, J., Lipofuscin and aging: a matter of toxic waste. *Sci. Aging Knowledge Environ.* 2005, DOI: 10.1126/sageke.2005.5.re1.

[14] Nilsson, E., Yin, D., Preparation of artificial ceroid/lipofuscin by UV-oxidation of subcellular organelles. *Mech. Ageing Dev.* 1997, *99*, 61–78.

[15] Samorajski, T., Keefe, J. R., Ordy, J. M., Intracellular localization of lipofuscin age pigments in the nervous system. *J. Gerontol.* 1964, *19*, 262–276.

[16] Feeney, L., Lipofuscin and melanin of human retinal pigment epithelium. Fluorescence, enzyme cytochemical, and ultrastructural studies. *Invest. Ophthalmol. Vis. Sci.* 1978, *17*, 583–600.

[17] Essner, E., Novikoff, A. B., Localization of acid phosphatase activity in hepatic lysosomes by means of electron microscopy. *J. Biophys. Biochem. Cytol.* 1961, *9*, 773–784.

[18] Ju, S.-J., Secor, D. H., Harvey, H. R., Growth rate variability and lipofuscin accumulation rates in the blue crab *Callinectes sapidus*. *Mar. Ecol. Prog. Ser.* 2001, *224*, 197–205.

[19] Munnell, J. F., Getty, R., Rate of accumulation of cardiac lipofuscin in the aging canine. *J. Gerontol.* 1968, *23*, 154–158.

[20] Strehler, B. L., Mark, D. D., Mildvan, A. S., Gee, M. V., Rate and magnitude of age pigment accumulation in the human myocardium. *J Gerontol* 1959, *14*, 430–439.

[21] Mann, D. M., Yates, P. O., Stamp, J. E., The relationship between lipofuscin pigment and ageing in the human nervous system. *J. Neurol. Sci.* 1978, *37*, 83–93.

[22] Kurz, T., Eaton, J. W., Brunk, U. T., Redox activity within the lysosomal compartment: implications for aging and apoptosis. *Antioxid. Redox Signal* 2010, *13*, 511–523.

[23] Weimer, J. M., Kriscenski-Perry, E., Elshatory, Y., Pearce, D. A., The neuronal ceroid lipofuscinoses: mutations in different proteins result in similar disease. *Neuromolecular Med.* 2002, *1*, 111–124.

[24] Santavuori, P., Haltia, M., Rapola, J., Raitta, C., Infantile type of so-called neuronal ceroid-lipofuscinosis. 1. A clinical study of 15 patients. *J. Neurol. Sci.* 1973, *18*, 257–267.

[25] Haltia, M., Rapola, J., Santavuori, P., Keranen, A., Infantile type of so-called neuronal ceroid-lipofuscinosis. 2. Morphological and biochemical studies. *J. Neurol. Sci.* 1973, *18*, 269–285.

[26] Haltia, M., Rapola, J., Santavuori, P., Infantile type of so-called neuronal ceroid-lipofuscinosis. Histological and electron microscopic studies. *Acta. Neuropathol.* 1973, *26*, 157–170.

[27] Shamsi, F. A., Boulton, M., Inhibition of RPE lysosomal and antioxidant activity by the age pigment lipofuscin. *Invest. Ophthalmol. Vis. Sci.* 2001, *42*, 3041–3046.

[28] Terman, A., Abrahamsson, N., Brunk, U. T., Ceroid/lipofuscin-loaded human fibroblasts show increased susceptibility to oxidative stress. *Exp. Gerontol.* 1999, *34*, 755–770.

[29] Luibl, V., Isas, J. M., Kayed, R., Glabe, C. G. et al., Drusen deposits associated with aging and age-related macular degeneration contain nonfibrillar amyloid oligomers. *J. Clin. Invest.* 2006, *116*, 378–385.

[30] Braak, H., Braak, E., Neuropathological staging of Alzheimer-related changes. *Acta. Neuropath.* 1991, *82*, 239–259.

[31] Mirra, S. S., Heyman, A., McKeel, D., Sumi, S. M. et al., The consortium to establish a registry for Alzheimer's disease (CERAD). Part II. Standardization of the neuropathologic assessment of Alzheimer's disease. *Neurology* 1991, *41*, 479–486.

[32] Boulton, M., Marshall, J., Repigmentation of human retinal pigment epithelial cells in vitro. *Exp. Eye Res.* 1985, *41*, 209–218.

[33] UniProt-Consortium, Ongoing and future developments at the Universal Protein Resource. *Nucleic Acids Res.* 2011, *39*, D214–D219.

[34] Keller, A., Nesvizhskii, A. I., Kolker, E., Aebersold, R., Empirical statistical model to estimate the accuracy of peptide identifications made by MS/MS and database search. *Anal. Chem.* 2002, *74*, 5383–5392.

[35] Nesvizhskii, A. I., Keller, A., Kolker, E., Aebersold, R., A statistical model for identifying proteins by tandem mass spectrometry. *Anal. Chem.* 2003, *75*, 4646–4658.

[36] Huang da, W., Sherman, B. T., Lempicki, R. A., Bioinformatics enrichment tools: paths toward the comprehensive functional analysis of large gene lists. *Nucleic Acids Res.* 2009, *37*, 1–13.

[37] Huang da, W., Sherman, B. T., Lempicki, R. A., Systematic and integrative analysis of large gene lists using DAVID bioinformatics resources. *Nat. Protoc.* 2009, *4*, 44–57.

[38] Terman, A., Kurz, T., Navratil, M., Arriaga, E. A. et al., Mitochondrial turnover and aging of long-lived postmitotic cells: the mitochondrial-lysosomal axis theory of aging. *Antioxid. Redox Signal* 2010, *12*, 503–535.

[39] Zhang, K., Sejnowski, T. J., A universal scaling law between gray matter and white matter of cerebral cortex. *Proc. Natl. Acad. Sci. USA* 2000, *97*, 5621–5626.

[40] Stadtman, E. R., Protein oxidation and aging. *Science* 1992, *257*, 1220–1224.

[41] Shimokawa, I., Higami, Y., Horiuchi, S., Iwasaki, M. et al., Advanced glycosylation end products in adrenal lipofuscin. *J. Gerontol. A Biol. Sci. Med. Sci.* 1998, *53*, B49–B51.

[42] Brownlee, M., Advanced protein glycosylation in diabetes and aging. *Annu. Rev. Med.* 1995, *46*, 223–234.

[43] Schutt, F., Bergmann, M., Holz, F. G., Kopitz, J., Proteins modified by malondialdehyde, 4-hydroxynonenal, or advanced glycation end products in lipofuscin of human retinal pigment epithelium. *Invest. Ophthalmol. Vis. Sci.* 2003, *44*, 3663–3668.

[44] Esterbauer, H., Schaur, R. J., Zollner, H., Chemistry and biochemistry of 4-hydroxynonenal, malonaldehyde and related aldehydes. *Free Radic. Biol. Med.* 1991, *11*, 81–128.

[45] Requena, J. R., Fu, M. X., Ahmed, M. U., Jenkins, A. J. et al., Quantification of malondialdehyde and 4-hydroxynonenal adducts to lysine residues in native and oxidized human low-density lipoprotein. *Biochem. J.* 1997, *322*(Pt 1), 317–325.

[46] Terman, A., Gustafsson, B., Brunk, U. T., The lysosomal-mitochondrial axis theory of postmitotic aging and cell death. *Chem. Biol. Interact.* 2006, *163*, 29–37.

[47] Sen, N., Hara, M. R., Kornberg, M. D., Cascio, M. B. et al., Nitric oxide-induced nuclear GAPDH activates p300/CBP and mediates apoptosis. *Nat. Cell Biol.* 2008, *10*, 866–873.

[48] Nakajima, H., Amano, W., Kubo, T., Fukuhara, A. et al., Glyceraldehyde-3-phosphate dehydrogenase aggregate formation participates in oxidative stress-induced cell death. *J. Biol. Chem.* 2009, *284*, 34331–34341.

[49] Petrak, J., Ivanek, R., Toman, O., Cmejla, R. et al., Deja vu in proteomics. A hit parade of repeatedly identified differentially expressed proteins. *Proteomics* 2008, *8*, 1744–1749.

[50] Guo, J., Prokai-Tatrai, K., Nguyen, V., Rauniyar, N. et al., Protein targets for carbonylation by 4-hydroxy-2-nonenal in rat liver mitochondria. *J. Proteomics* 2011, *74*, 2370–2379.

[51] Pamplona, R., Dalfo, E., Ayala, V., Bellmunt, M. J. et al., Proteins in human brain cortex are modified by oxidation, glycoxidation, and lipoxidation. Effects of Alzheimer disease and identification of lipoxidation targets. *J. Biol. Chem.* 2005, *280*, 21522–21530.

[52] Chung, W. G., Miranda, C. L., Maier, C. S., Detection of carbonyl-modified proteins in interfibrillar rat mitochondria using N'-aminooxymethylcarbonylhydrazino-D-biotin as an aldehyde/keto-reactive probe in combination with Western blot analysis and tandem mass spectrometry. *Electrophoresis* 2008, *29*, 1317–1324.

[53] Kominami, E., Ezaki, J., Muno, D., Ishido, K. et al., Specific storage of subunit c of mitochondrial ATP synthase in lysosomes of neuronal ceroid lipofuscinosis (Batten's disease). *J. Biochem.* 1992, *111*, 278–282.

[54] Ezaki, J., Tanida, I., Kanehagi, N., Kominami, E., A lysosomal proteinase, the late infantile neuronal ceroid lipofuscinosis gene (CLN2) product, is essential for degradation of a hydrophobic protein, the subunit c of ATP synthase. *J. Neurochem.* 1999, *72*, 2573–2582.

